Available online at www.sciencedirect.com
ScienceDirect
Acta Materialia 55 (2007) 2791–2803
Acta MATERIALIA
www.actamat-journals.com

Effects of segregating elements on the adhesive strength and structure of the α-Al_2O_3/β-NiAl interface

Karin M. Carling [1], Emily A. Carter *

Department of Mechanical and Aerospace Engineering and Program in Applied and Computational Mathematics, Princeton University, Princeton, NJ 08544-5263, USA

Received 14 August 2006; received in revised form 9 November 2006; accepted 3 December 2006
Available online 26 February 2007

Abstract

We investigate with first-principles density functional theory (DFT) the adhesion of the $Al_2O_3(0001)$/NiAl(110) interface as a model for the thermally grown oxide/bond coat alloy interface in thermal barrier coatings. We find that the clean interface has an ideal work of adhesion of 0.66 J m^{-2}. We predict that S impurities reduce interfacial adhesion significantly, due to a reduction in cross-interface bonds. The presence of Pt alters the interface adhesion only slightly, while Hf dopants dramatically increase adhesion via formation of strong Hf–O bonds, as expected from Hf's open-shell character. We discuss the implications of these predictions, which are consistent with experimental observations of the effects of S, Pt, and Hf on the lifetime of thermal barrier coatings.

Keywords: Nickel aluminides; Crystalline oxides; Interface structure; Interface segregation; Density functional

1. Introduction

In many technological applications, coatings are used to protect component materials from harsh environments. For example, thermal barrier coatings (TBCs) are used in jet turbine engines so that the engine may operate at higher temperatures, providing either higher thrust and/or better fuel efficiency. TBCs generally consist of a multi-layered structure containing a topcoat of yttria-stabilized zirconia (YSZ) that provides thermal protection up to ~1600 °C, a thermally grown oxide (TGO) layer of alumina that limits oxidation and corrosion, and a NiAl-based bond coat alloy in contact with the metal engine component. Optimized bond coat alloys typically contain various additives, such as Co, Cr or Pt, and reactive elements (REs) such as Y and Hf [1,2].

The service lifetime of a TBC is strongly affected by thermal cycling of the engine, which eventually causes the coating to spall. Often the failure appears to occur along the bond coat alloy/TGO interface [3], by nucleation of small cracks and voids at defects, which then coalesce, leading eventually to large-scale buckling and spallation [4]. To avoid spallation and failure of the TBC, it is important to improve the adhesion between the layers in the structure, in particular the adhesion of what appears to be the weak link, namely the bond coat alloy/TGO interface.

It is difficult to investigate the layered TBC structure experimentally in situ, and although post-mortem microscopy studies on thermally cycled TBCs have been reported [3], interpretations of these remain controversial. Therefore, it is still unclear which of the proposed failure modes lead to spallation, which impurities accelerate failure, and which additives are responsible for delaying spallation. As a result, theoretical calculations may prove helpful in isolating causes of failure and origins of enhanced lifetime. In particular, predictive models such as those based on first-principles density functional theory (DFT)

* Corresponding author. Tel.: +1 609 258 5391; fax: +1 609 258 5877.
E-mail address: eac@princeton.edu (E.A. Carter).
[1] Present address: Department of Mechanical and Materials Engineering, Faculty of Technology and Science, Karlstad University, SE-651 88 Karlstad, Sweden.

1359-6454/$30.00
doi:10.1016/j.actamat.2006.12.020

calculations [5,6] may be able to shed light on atomic-scale aspects of the problem.

Sulfur impurities have been found to segregate to the bond coat/oxide scale interface, concomitant with void formation [7,8], and a weakening of the interface [4,9–12]. To avoid this detrimental effect on the interface, strategies are employed to lower the S content in the metal substrate and bond coat alloys [2], either by treatment with hydrogen [9], adding REs that may "getter" the S so it does not segregate to the interface [4,13,14], or using Pt–aluminide bond coats, whose S content actually might be higher than that in the conventional NiCrAlY coatings, but Pt seems to inhibit S segregation to the interface and the associated void formation [15]. The actual means by which these approaches affect the lifetime of the TBC is quite controversial; all that is known is that S segregation to the oxide scale/bond coat interface is inhibited [7,14]. A rather low-level local density approximation (LDA) pseudopotential DFT calculation suggested recently that adhesion decreases significantly when S is introduced into the $Al_2O_3(0001)$/Ni(111) interface [16]. Here we utilize all-electron DFT-GGA (generalized gradient approximation) calculations to examine how S affects the α-$Al_2O_3(0001)$/β-NiAl(110) interface.

Recently, Pt–aluminide bond coat alloys based on single-phase β-NiAl, with Pt substituting for Ni, have come into use [2,4]; this Pt addition gives the NiAl alloy excellent corrosion resistance. Upon thermal cycling of a TBC with a PtNiAl bond coat, transmission electron microscopy (TEM) analysis finds a stable α-Al_2O_3 scale [17], which is thought to be associated with extending the TBC lifetime. The role of Pt is still very unclear: Pt improves scale adhesion, but does not change the microstructure of the alumina scale [18] or the oxidation kinetics [15], nor does it segregate to alumina grain boundaries [10], while REs added to the NiCrAlY-based bond coat do all of the above [14]. It has been shown that Pt suppresses formation of spinel oxide phases on both NiAl model alloys and commercial coatings [19]. These spinels are usually brittle and may be a source of de-adhesion. In the present work, we examine the effect of Pt on the α-Al_2O_3/β-NiAl interfacial adhesion.

Adding reactive elements, such as Y, Hf and Zr, to traditional bond coats slows down the growth of the oxide scale [14], and enhances adhesion, especially in NiAl bond coats [2,20]. It is also known that these REs can form "oxide pegs", the usefulness of which has been debated in the literature [13]. Some assert that these pegs arrest crack propagation [1,14,21,22], while others believe they do not relieve stress [23] and could be a source of brittleness. The actual means by which REs affect the lifetime of TBCs is quite controversial. In previous first-principles calculations, it was shown that early transition metals can significantly improve the adhesion between Ni and Al_2O_3 [24,25]. This increased adhesion was suggested to arise from the open-shell electronic structure of the early transition metals, which enhances the bonding between the highly ionic Al_2O_3 and the metal substrate. In the current work, we examine how Hf affects Al_2O_3/NiAl interface adhesion, since Hf is one of the most common reactive elements added to TBC bond coats [26].

In this paper, we investigate the bonding on the atomic scale of the $Al_2O_3(0001)$/NiAl(110) interface, and how this bonding is affected by the addition of small amounts (0.1 ML) of S, Pt and Hf at the interface. We begin with a description of the first-principles method we use and our strategy for calculating properties of interest. We then discuss results for the clean $Al_2O_3(0001)$/NiAl(110) interface, followed by a presentation of results for this interface with S, Pt and Hf. Finally, we discuss our predictions and their implications for TBC adhesion and lifetime, and summarize our conclusions.

2. Method

We employ the VASP implementation [27–29] of spin-polarized periodic density functional theory (DFT) within a plane-wave basis [5,6]. The Perdew–Burke–Ernzerhof (PBE) version [30] of the GGA for electron exchange and correlation is used. The interactions between the valence electrons and the nuclei plus core electrons is described by projector augmented wave (PAW) potentials [31,32] for all elements. PAW is an all-electron DFT method within the frozen core approximation. We use a kinetic energy cutoff of 400 eV for the plane wave basis, which yields an absolute total energy convergence of 0.02 eV/atom for the NiAl(110), $Al_2O_3(0001)$ and interface slabs. Sampling in k-space is done with a gamma-point centered Monkhorst–Pack grid [33] of $4\times10\times1$ points, which yields 22 points in the irreducible Brillouin zone. This leads to an absolute total energy convergence of 1 meV/atom or better for the metal–oxide interface and isolated metal or oxide slabs. The integration of the Brillouin zone is done with the Methfessel–Paxton method [33], with a Fermi surface smearing width of 0.1 eV.

The periodic cell of the interface is built from one NiAl(110) slab and one $Al_2O_3(0001)$ slab with an interface area of 59.3 Å^2, and one dopant/impurity atom per periodic cell (0.1 ML) is inserted at the interface as an adsorbate on the NiAl surface. This low dopant/impurity coverage was employed for two reasons: (i) any effects seen at this low coverage would be expected simply to increase as the coverage increased and (ii) it is thought that a typical coverage of segregating element at these interfaces is no more than ~0.2 ML [14]. The periodic images of the interface slab are separated with at least 12 Å of vacuum. The NiAl(110) surface, which is the closest-packed and most stable surface of β-NiAl, is modeled by a slab consisting of five layers with 10 atoms (five Ni and five Al) per layer. The two layers farthest away from the oxide coating are kept fixed at their bulk positions to mimic a semi-infinite crystal. We consider the closest-packed and most stable surface of α-Al_2O_3, namely $Al_2O_3(0001)$, as the oxide coating that grows at high temperatures on NiAl. We represent

this $Al_2O_3(0001)$ coating by a slab that is three Al–O_3–Al layers thick, and the slab is cut such that both bulk truncated surfaces end with Al atoms. It has been shown in earlier work that this is the most stable termination of Al_2O_3 [34–36], and it is known that alumina formed via oxidation of the metal substrate tends to grow in with surfaces parallel to the (0001) planes [37]. Each layer of the slab consists of three Al_2O_3 formula units, i.e. the full slab consists of 27 O and 18 Al atoms. We choose to use a three-layer thick $Al_2O_3(0001)$ slab based on layer thickness convergence tests of the structure of Al_2O_3 on the structurally similar substrate FeAl [38], where it was shown that a three-layer $Al_2O_3(0001)$ coating on the metal substrate was the thinnest slab that still has the structure of α-Al_2O_3 after full relaxation. For the $Al_2O_3(0001)$/Ni(111) interface, even a two-layer oxide coating was found to basically retain the oxygen planes from bulk alumina [36]. The misfit between these NiAl and Al_2O_3 surfaces is 3%, with Al_2O_3 under slight compression.

Structural relaxation of ion positions is done in steps in order to enhance convergence. First, only relaxation along the direction of the interface normal is allowed until the forces along the interface normal are less than 1 eV $Å^{-1}$. We then allow full relaxation of all atoms until the forces on the relaxing atoms are less than 0.08 eV $Å^{-1}$, except for the two bottom layers of the NiAl substrate as noted above. As a final step, we change from the conjugate gradient minimization algorithm to the quasi-Newton algorithm and relax the ion positions until all forces are less than 0.05 eV $Å^{-1}$.

We define the ideal work of adhesion as $W_{ad} = E_{NiAl/X} + E_{Al_2O_3} - E_{NiAl/X/Al_2O_3}$, where the E_i's are the respective PAW-DFT-GGA total energies of the slabs indicated. For the NiAl/X and NiAl/X/Al_2O_3 slabs, the PAW-DFT-GGA equilibrium lattice vectors for bulk NiAl were employed, while the alumina slab was calculated either with the bulk NiAl lattice vectors (to eliminate elastic strain energy artifacts upon relaxation) or with PAW-DFT-GGA equilibrium lattice vectors for bulk α-Al_2O_3. These two limits give some idea of bounds on W_{ad}. By ideal work of adhesion, we refer to the energy required to separate the interface into two materials, neglecting plasticity. While this should engender little error for the brittle Al_2O_3 coating, which will not deform plastically, metallic NiAl is expected to form dislocations upon tensile loading, which will increase the work of adhesion considerably via energy dissipation as the dislocations form and move. Typical distances between dislocations are of the order of a micron; our DFT calculations necessarily consider length scales incompatible with dislocation formation and motion. As a result, one can only consider this non-plastic contribution to the work of adhesion within DFT. Nevertheless, trends in this intrinsic ideal work of adhesion appear to correlate well with empirically observed trends in stability of various interfaces [39].

Electron density changes upon formation of the interface were calculated from $\Delta\rho = \rho_{NiAl/X/Al_2O_3} - \rho_{NiAl/X} - \rho_{Al2O3}$, where the NiAl/X and Al_2O_3 slabs used to calculate $\Delta\rho$ were constructed by removing from the relaxed interface structures all atoms that do not belong to either NiAl/X or Al_2O_3, respectively. Then we solve for the density appropriate for the atoms in the separated slabs, which are frozen in the relaxed interface atomic positions. The grid for the electron density was fixed to $160 \times 64 \times 392$ points in all cells. Positive $\Delta\rho$ indicates accumulation of charge density upon interface formation; negative $\Delta\rho$ indicates depletion.

The projected density of states (PDOS) for atoms at the interface were calculated by projection onto atomic states within a Wigner–Seitz sphere around each atom, as implemented in VASP. We used the following atomic radii: 0.604 Å for O, 1.432 Å for Al, 1.246 Å for Ni, 1.025 Å for S, 1.388 Å for Pt, and 1.564 Å for Hf. We chose to use atomic radii in order to be able to compare these data with our previous work examining adsorption of these segregating elements onto NiAl(110) [40]. We caution that interpretation of these projections can only be trusted in a qualitative sense due to the numerical approximations employed and the somewhat arbitrary choice of cutoff radii.

3. Results

3.1. Clean Al_2O_3/NiAl interface

The information provided above does not completely define the structure of the interface, because we must still determine the most favorable positions of the atoms in the alumina slab with respect to the underlying NiAl(110) substrate. Thus, we investigated four relative translations of the Al_2O_3 slab for the clean (i.e. no segregating elements present) $Al_2O_3(0001)$/NiAl(110) interface. First, we took the bulk-terminated slabs and put them together without any adjustment in the lateral direction, i.e. no translation. This interface turned out to give a very low work of adhesion. Therefore, three translations of the oxide layer were considered, where we determined that the position of the Al outer half-layer of the oxide with respect to the NiAl surface was the important factor. The first translation aimed to put as many Al atoms from the outer half-layer of alumina in three-fold hollow sites of the 2Ni–Al type (i.e. 2 Ni atoms and 1 Al atom comprising the three-fold site). The second translation focused on maximizing the number of Al atoms from the outer half-layer of alumina in the other type of three-fold site found on the NiAl(110) surface, namely the Ni–2Al site (defined similarly). The third translation maximized the number of the Al half-layer atoms in Ni–Ni bridge sites on the NiAl(110) substrate.

Table 1 displays the ideal work of adhesion for these translations, considering a final state in which the isolated Al_2O_3 slab is in either an unstrained or strained (compressed to adopt the NiAl lattice constant) state. The unstrained adhesion energies could be considered lower

Table 1
The work of adhesion $E_{adhesion} = (E_{NiAl} + E_{Al_2O_3}) - E_{interface}$ for the clean and doped $Al_2O_3(0001)$/NiAl(110) interfaces[c]

Translation/system[b]	Al_2O_3 unstrained[a] (J m^{-2})	Al_2O_3 strained[a] (J m^{-2})
No translation	−0.663	0.014
Ni–2Al three-fold	−0.181	0.496
2Ni–Al three-fold	−0.136	0.541
Ni–Ni bridge	−0.016	0.661
S-doped	−0.482	0.181
Pt-doped	−0.130	0.533
Hf-doped	1.393	2.056

[a] The isolated oxide slab is relaxed either with lattice parameters from the interface cell, i.e. the NiAl(110) lattice parameters ("Al_2O_3 strained"), or with the Al_2O_3 bulk lattice parameters ("Al_2O_3 unstrained").
[b] Four different lateral translations of the oxide with respect to the NiAl substrate are considered (see text for details).
[c] Large positive values correspond to a stable interface.

bounds, but the fact that some are unphysical (negative values) indicates that allowing for elastic strain energy release is not sensible. Henceforth, we focus on the adhesion energies where the strain energy (an extensive quantity that we cannot properly account for anyway) is kept constant, i.e. the right-hand column of Table 1. From these data, we see that the closer the Al half-layer of the oxide is positioned along the Ni rows of the NiAl substrate, the stronger the adhesion. The third translation, which put the half-layer Al atoms from the oxide in, or close to, Ni–Ni bridge sites on the NiAl(110) surface, i.e. in positions along the Ni rows, gives the strongest adhesion of the oxide. Therefore, we focused our subsequent analysis on this structure. That Al atoms from the oxide prefer positions along Ni rows has been observed by scanning tunneling microscopy (STM) and confirmed by other DFT calculations [41].

The adhesion energy of the clean interface, 0.661 J m^{-2}, is similar to the one predicted for the $Al_2O_3(0001)$/Ni(111) interface [36], where the adhesion energy for the same thickness of alumina was found to be 0.456 J m^{-2}. The systems have a similar lattice mismatch, 3%, and given that the nearest-neighbor interactions for both interfaces involve Ni from the substrate and Al from the alumina, it makes sense that the W_{ad}'s are similar. In both interfaces, the oxygen planes of the three-layer alumina slab maintain their bulk shape as flat and hexagonal, suggesting that this may be a reasonable structural model to mimic the actual microns-thick alumina coating.

The structure of the fully relaxed interface is shown in Fig. 1a. The Al atoms from the NiAl substrate appear to form bonds with O atoms in alumina (Al_{NiAl}–O), while Ni atoms appear to form bonds with the Al atoms in the oxide (Ni–$Al_{Al_2O_3}$). Table 2 lists the bond lengths between atoms in the metal and the oxide. Consistent with the qualitative evidence of Fig. 1, Table 2 quantifies that the bond-

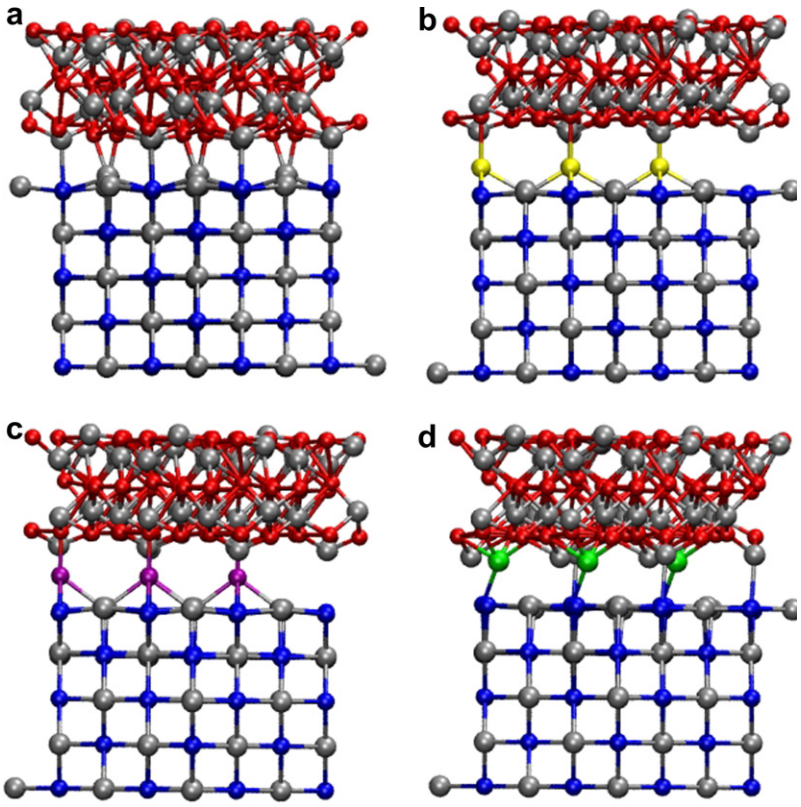

Fig. 1. Optimized structures of the interfaces: (a) the clean Al_2O_3/NiAl interface, (b) the Al_2O_3/S/NiAl interface, (c) the Al_2O_3/Pt/NiAl interface and (d) the Al_2O_3/Hf/NiAl interface. Ni is blue, Al is grey, O is red, S is yellow, Pt is purple, and Hf is green. The cutoff for the bonds shown in the figure is 2.6 Å. (For interpretation of the references to colour in this figure legend, the reader is referred to the web version of this article.)

Table 2
The distances (in Å) between atoms in the clean and doped interfaces

Bond	Interface dopant "X"			
	None	S	Pt	Hf
"X"–O	–	**2.42**, 3.21, 3.33	**2.07**, 3.12, 3.27	**1.87**, **1.89**, **2.34**, **2.44**
"X"–$Al_{Al_2O_3}$	–	3.33	3.28, 3.37	2.93
"X"–Ni	–	**2.19**, **2.21**	**2.39**, **2.47**	**2.43**, 2.68
"X"–Al_{NiAl}	–	**2.37**, **2.37**	**2.45**, **2.46**	2.78, 3.49
Ni–O	2.92	–	–	3.36, 3.45, 3.47, 3.50
Al_{NiAl}–O	**1.98, 2.01**, 2.83	3.34, 3.46, 3.46	3.48	3.38, 3.42, 3.48
Ni–$Al_{Al_2O_3}$	**2.43, 2.44**, **2.70**, 2.83	**2.86**, 3.16, 3.43	**2.88**, **3.18**, 3.43	**2.45**, 2.65, 2.74
Al_{NiAl}–$Al_{Al_2O_3}$	2.82, 2.83	3.50	3.48	3.49
Bonds/nm^2	8.4	1.7	5.1	10.1
Adhesion (J m^{-2})	0.661	0.181	0.533	2.056

All distances less than 3.0 Å for the clean Al_2O_3/NiAl interface and less than 3.5 Å for the S-, Pt- and Hf-doped interfaces are listed.
The distances in bold type highlight either the shortest bonds or the bonds in the interface structures appearing in the charge density difference maps (Figs. 2–6).

ing across the interface is dominated by Al_{NiAl}–O and Ni–$Al_{Al_2O_3}$ bonds, as shown by the bold-faced values for the shortest bonds across the interface. In particular, the clean interface has shortest bonds (only ~2 Å) between two Al from the NiAl substrate and two O from the oxide. The next shortest bonds are found between Ni from the substrate and Al from the oxide (~2.4 Å). All other cross-interface bonds are longer than 2.5 Å. In bulk NiAl, the Ni–Al bond is 2.5 Å and for bulk Al_2O_3 the shortest Al–O bond is 1.9 Å. Thus, the cross-interface bonds are very similar in length to the corresponding bonds in the bulk crystals.

To enhance our understanding of the bonding across the interface, electron density difference maps are shown in Figs. 2 and 3. The change in the electron density upon formation of the clean interface is dominated by the Al_{NiAl}–O and Ni–$Al_{Al_2O_3}$ interactions, in agreement with the bond length data. Fig. 2 focuses on cuts through an Al in Al_2O_3 at the interface and shows an accumulation of charge between the Ni and Al atoms across the interface, suggesting formation of metallic bonds. Fig. 3 exhibits cuts through an O atom in Al_2O_3 at the interface and suggests a transfer of charge occurs from the Al of NiAl to the O atom, consistent with formation of an ionic Al–O bond. In all, we conclude that there are five bonds formed across the interface in each cell (2 Al–O and 3 Ni–Al), which corresponds to a "bond density" of 8.4 bonds nm^{-2}.

In order to investigate the nature of the bonding across the interface further, we calculated the local density of states (LDOS), shown in Fig. 4, for an O and a Ni atom involved in bonding to Al atoms across the interface. Al LDOSs are not shown because the amplitudes for all Al LDOSs are very small and not informative (this is due to the ionic nature of Al in alumina and to the delocalization of Al's electrons in NiAl, which is not captured well by the Wigner–Seitz radius employed in the LDOS analysis). The occupied states of the O atom are shifted down relative to the isolated alumina slab, indicating a stabilization of the O valence states, which would occur upon electron transfer from Al to O. The LDOS for the Ni atom does not give any indication of the type of bond that might be formed with the Al from the oxide, although the states are slightly shifted down compared to the LDOS of Ni atom at the clean NiAl(1 1 0) surface.

Next, we consider in turn how the clean interface is affected by the presence of S impurities and Pt and Hf dopants. The most stable translation for the clean Al_2O_3/NiAl interface discussed above is our starting point for these calculations with impurity or dopant atoms segregated to the interface.

3.2. Sulfur impurities at the interface

From our previous work [40], we determined that the preferred adsorption site for S on the NiAl(1 1 0) surface is the 2Ni–Al three-fold site. Therefore, we use that site as the initial position for the sulfur with respect to the NiAl substrate. There are 10 of these initial sites in the interface cell, and we choose the one farthest away from all the Ni–$Al_{Al_2O_3}$ cross-interface bonds that occur in the clean interface geometry, in order to disrupt as little as possible the Ni–Al bonding across the interface. However, this choice puts one of the O atoms from the oxide on top of the S atom in the initial guess structure. While we cannot exclude the possibility that other initial positions for the S atom might produce a lower energy structure, we will see below that in the case of Hf, this analogous initial guess structure did not prevent large movements of Hf to a more favorable location. Thus, if the initial S position is terribly unfavorable, it is clear that there is room for the much smaller S atom to readjust at the interface. Given the significant expense of these structural relaxations, we therefore did not pursue other initial guess structures.

The structure of the fully relaxed interface is shown in Fig. 1b. By comparison with the clean interface, the optimal gap between the two materials has increased considerably, which is to be expected since the S atom is intercalated into the interface. This is also consistent with post-mortem transmission electron microscopy pictures that show S present in voids that have formed at the

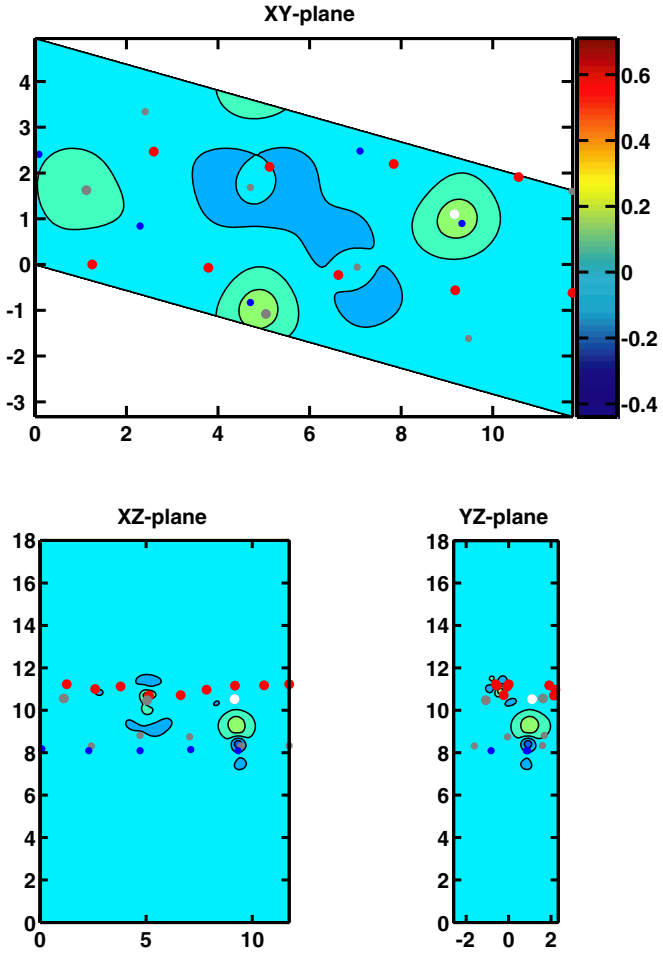

Fig. 2. Electron density difference maps for three cuts through the Al_2O_3/NiAl interface. The white dot marks an Al atom from the oxide that bonds to a Ni from the metal substrate. The dots mark the positions of the atoms in the oxide and substrate layers closest to the interface. Red is oxygen, blue is nickel, large grey is Al from the oxide, small grey is Al from the NiAl. The top panel shows the cut between the Al and the Ni parallel to the interface plane. The two lower panels show cuts perpendicular to the interface through the Al atom. (For interpretation of the references to colour in this figure legend, the reader is referred to the web version of this article.)

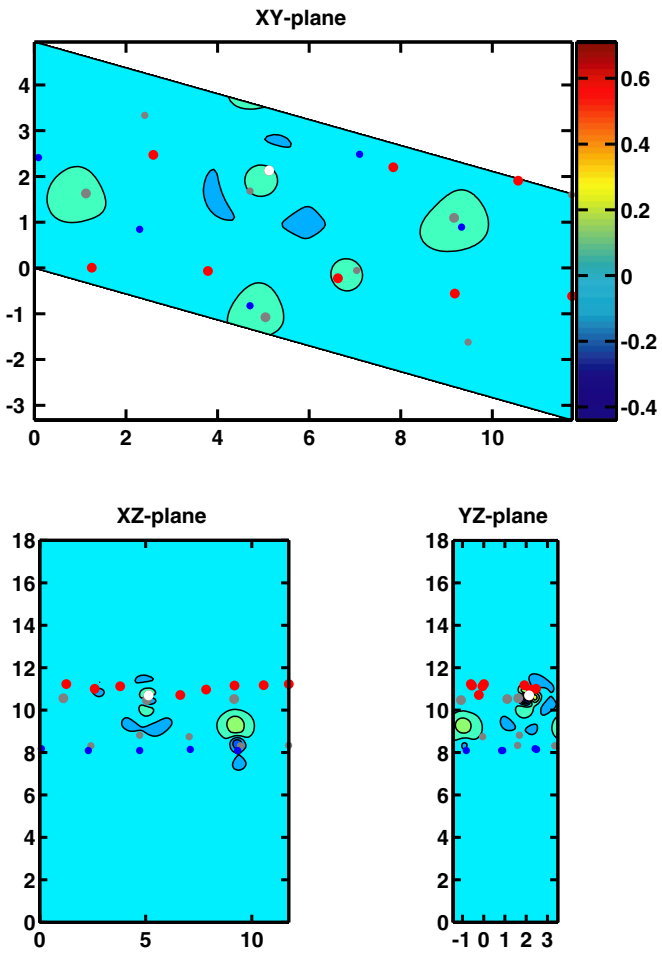

Fig. 3. Electron density difference maps for three cuts through the Al_2O_3/NiAl interface. The white dot marks an O atom from the oxide that bonds to an Al from the metal substrate. The dots mark the positions of the atoms in the oxide and substrate layers closest to the interface. Red is oxygen, blue is nickel, large grey is Al from the oxide, small grey is Al from the NiAl. The top panel shows the cut between the O and the Al parallel to the interface plane. The two lower panels show cuts perpendicular to the interface through the O atom. (For interpretation of the references to colour in this figure legend, the reader is referred to the web version of this article.)

interface between the NiAl bond coat alloy and the thermally grown oxide, Al_2O_3 [7,8]. Those microscopy images suggest that S acts to debond the Al_2O_3 from the bond coat alloy. Indeed, the only "bond" that appears to form across the interface containing S is between S and O; the nature of this "bond" is discussed further below. Table 2 lists the bond lengths between S and atoms from the metal and the oxide. The S atom appears to have four close contacts with the metal and one with the oxide, i.e. the S atom moved from the initial 2Ni–Al adsorption site to the nearby four-fold-coordinated long-bridge site where it has two Ni atoms as its nearest neighbors. Presumably, the S moved to this site to minimize repulsions with the O from Al_2O_3. This puts the S atom in the position where an Al atom would be if the NiAl(1 1 0) surface was growing epitaxially. The S–O "bond" distance is 2.42 Å, which is much larger than a typical single S–O bond length, e.g. 1.57 Å in the molecule H_2SO_4 [42]. There is also a significant increase in the distances between the atoms from the oxide and the metal to the point that only one metal–oxide Ni–Al atom pair has a "bond distance" within 3 Å. All of the cross-interface bonds have lengthened considerably compared to the clean interface.

As a result of the reduction in cross-interface Ni–Al bonds, we expect that the S impurity will reduce the interfacial adhesion energy. Indeed, Table 1 shows that the work of adhesion decreases by 0.48 J m^{-2} (73%) when S is added to the interface. Our prediction must be considered simply a qualitative trend, because the actual sulfur content at the interface may be larger or smaller than 0.1 ML. As the S concentration at the interface increases, however, we expect further reductions in the interfacial

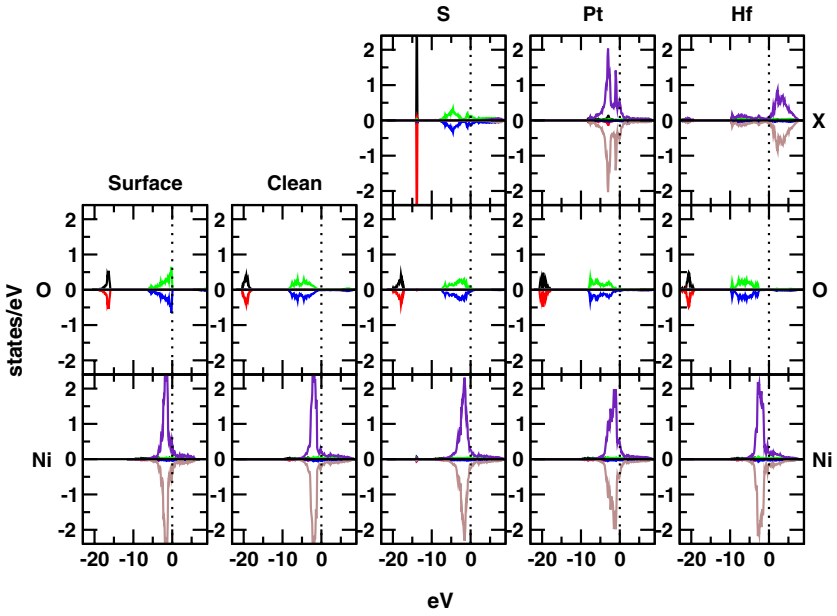

Fig. 4. Projected density of states for atoms from the isolated NiAl and Al_2O_3 surfaces, and the clean, S-, Pt- and Hf-doped interfaces. A surface atom (O or Ni) is shown for the isolated surfaces. For the clean interface, an O and a Ni involved in cross-interface bonds are shown. For the doped interfaces, the dopants and the O and Ni closest to the dopant are shown. Black is spin up s-states, red is spin down s-states, green is spin up p-states, blue is spin down p-states, indigo is spin up d-states, brown is spin down d-states. The vertical dotted line indicates the Fermi level. The down-spin densities of states are plotted as negative for clarity only; the actual DOS are of course the absolute values of these negative numbers. (For interpretation of the references to colour in this figure legend, the reader is referred to the web version of this article.)

adhesion. Although it is possible that there exists another, more favorable site for S to sit at the interface that might raise the adhesion energy, given that all other sites would be even closer to the Ni–Al cross-interface bonds, it is likely that any other site that we might consider as an initial guess would lead to a similar disruption of those cross-interface bonds.

The changes in the electron density upon formation of the interface containing S are shown in Fig. 5. There is a depletion of electrons around the S atom, as well as around the O atom with which the sulfur is interacting, as seen in the two cuts perpendicular to the interface through the S atom. It is likely that electron pair–electron pair repulsion exists between the O^{2-} of Al_2O_3 and the neutral S to begin with, which is subsequently reduced upon optimization both by movement of the S and redistribution of the electron density away from the S and O. We therefore conclude that these nearby S and O atoms in fact are not forming a bond at all. In the cut parallel to the interface, we see accumulation of electron density corresponding to a $Al_{Al_2O_3}$–Ni bond across the interface (here the bond length is 2.86 Å, quite close to the 2.88 Å Ni–Al distance in bulk NiAl [40]), indicating that this is a legitimate cross-interface bond. Thus, we conclude that only one true bond is present in our interface cell, corresponding to 1.7 bonds nm^{-2}.

Fig. 6 compares the LDOS for the S atom as an adsorbate on the NiAl(1 1 0) surface and as an impurity at the interface. We see that the S LDOS is more dispersed and is of smaller amplitude for S at the interface compared to as an adsorbate on NiAl(1 1 0). This is consistent with the electron density difference maps discussed above, where it is seen that S loses electron density and the density on S is more delocalized, in order to minimize repulsion with alumina's nearby oxygen atom. To investigate the effect of S on the atoms of the metal and the oxide, we display the LDOS for Ni and O in Fig. 4. While no significant changes in the LDOS for the Ni and O atoms are observed compared with their states for a clean interface, there is a slight destabilization and increased dispersion of the O states, which is consistent with the loss of electron density around the oxygen upon formation of the S-containing interface and with the S and O repulsion discussed above.

3.3. Platinum-doped interface

On the NiAl(1 1 0) surface, we found that Pt preferentially adsorbs on the Ni–Ni long-bridge site [40]; we therefore use this as the initial guess for the position of the Pt dopant with respect to the NiAl substrate. There are five of these initial sites in the interface cell; we choose the one farthest away from all the Ni–$Al_{Al_2O_3}$ cross-interface bonds, just as we did with the S atom. This produces a similar position as in the S case, with respect to the oxide, i.e. there is an O atom on top of the Pt in the initial guess structure. Again, our strategy in constructing an initial guess structure was to preserve Ni–$Al_{Al_2O_3}$ bonds while inserting the segregating element; of course this means we cannot be sure that there is not a lower energy interface structure with the Pt atom nearer to a Ni–$Al_{Al_2O_3}$ bond. We consider it to be unlikely, however, for the reasons argued above for S, and given the expense of these calculations, exploring other local minima is beyond the scope of this study.

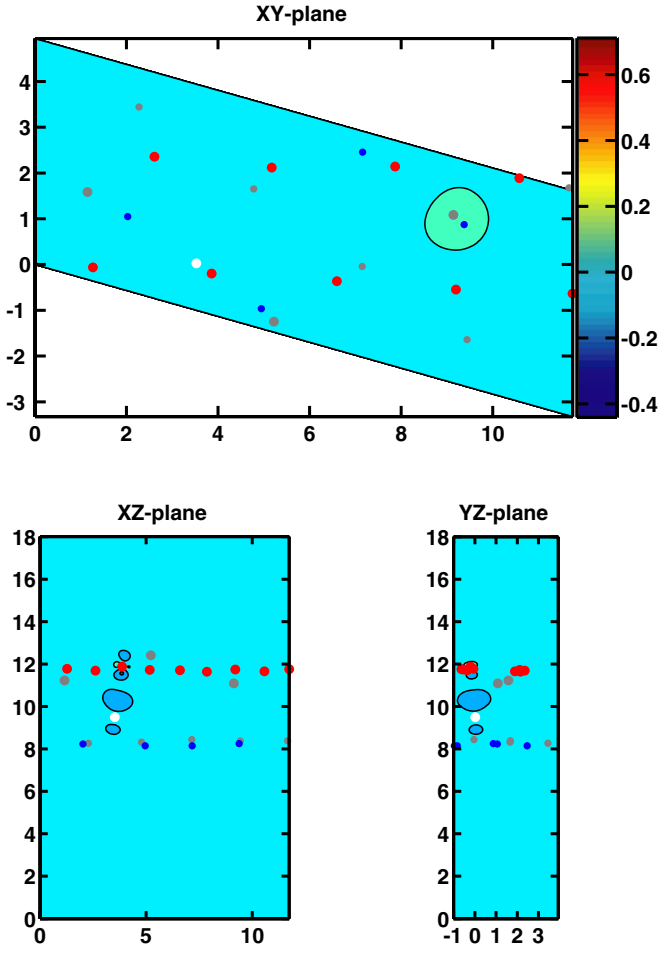

Fig. 5. Electron density difference maps for three cuts through the Al_2O_3/S/NiAl interface. The white dot marks the S atom. The dots mark the positions of the atoms in the oxide and substrate layers closest to the interface. Red is oxygen, blue is nickel, large grey is Al from the oxide, small grey is Al from the NiAl. The top panel shows the cut through the S atom parallel to the interface plane. The two lower panels show cuts perpendicular to the interface through the S atom. (For interpretation of the references to colour in this figure legend, the reader is referred to the web version of this article.)

Fig. 1c depicts the structure of the fully relaxed interface containing 0.1 ML Pt. Again, since Pt is intercalated at the interface, the gap between the metal and the oxide has increased compared to the clean interface. As with S, it appears that only one "bond" forms across the interface and it is between Pt and O. We investigate this "bond" further below. The bond lengths between Pt and atoms from the metal and the oxide are shown in Table 2. The Pt atom is shifted off the Ni–Ni long-bridge position, which is manifested in unequal bond distances to the two Ni atoms (2.39 and 2.47 Å). The shift is 0.11 Å in the plane parallel to the surface. That the Pt atom shifts off the Ni–Ni long-bridge site is likely due to the interaction with the O atom from the oxide; Pt moves away from the O atom during the relaxation. The Pt–O bond for O adsorbed on Pt(1 1 1) is ~2 Å [43], which is only slightly shorter than the distance we find here. Apart from the Pt–oxo bond, there is only one Ni–Al "bond" across the interface shorter than 3 Å, indicative of the increased gap between the metal substrate and the oxide coating. By comparison, the lengths of Ni–Al cross-interface bonds in the clean interface are considerably shorter, 2.43–2.70 Å.

The predicted ideal work of adhesion for the Pt-doped interface is 0.533 J m^{-2}, slightly larger than for the S-containing interface but slightly smaller than for the clean interface (Table 1). Again, electron density difference maps (Fig. 7) help reveal the reasons for the lack of strong adhesion. In the cut parallel to the interface, we see two areas of electron accumulation and a depletion of electrons at the Pt atom. The perpendicular contour plots of electron density changes show significant depletion of electrons both above and below the Pt atom in the shape of a dz^2 orbital, with a concomitant decrease of electron density around the O atom directly above the Pt. This suggests the Pt–O interaction was at least initially repulsive (due to the nearly-closed-shell Pt atom interacting with the effectively closed shell O^{2-}-like ion [24]). The Pt and O atoms try to minimize this interaction by transferring electron density to other parts of the interface, perhaps then allowing a more covalent bond to form. The two regions where electrons accumulate are two Ni–Al cross-interface pairs, with elongated Ni–Al bond lengths of 2.88 and 3.18 Å. The accumulation of charge between these pairs of atoms indicates that these bonds are retained across the interface, despite their elongation. Therefore, we conclude that there are three cross-interface bonds formed (two Ni–Al and one Pt–O) that bind the oxide to the metal in this cell, giving 5.1 bonds nm^{-2} for this interface, compared to 8.4 bonds nm^{-2} for the clean interface. The decrease in "bond density" and the elongated cross-interface bonds are probably responsible for the slightly weakened adhesion compared to the clean interface.

In order to explore further the nature of the bonds at the Pt-doped interface, we examine the LDOS for the atoms at this interface. Fig. 6 provides a comparison of the LDOS for Pt as an adsorbate on the NiAl(1 1 0) surface and as intercalated in the Al_2O_3/NiAl interface. The number of states for Pt at the interface declines, in line with the decrease in the electron density that is seen in the density difference plots. The LDOS for Pt and the Ni and O atoms that are its nearest neighbors are shown in Fig. 4. There are no significant changes in the states for the Ni and O atoms, as compared with their states for a clean interface. The loss of electron density around the O atom is seen as a slight decrease of the number of p-states close to the Fermi level, as well as an increased dispersion.

Up to this point, we have only considered Pt in an interstitial-like site between the oxide scale and the metal alloy. But Pt is known to be a substitutional impurity in NiAl, replacing Ni on the Ni sublattice [44]. Thus, while S and Hf are thought to segregate to grain boundaries as we have modeled them here, Pt may not segregate to the hetero-interface but instead simply may be present at the interface

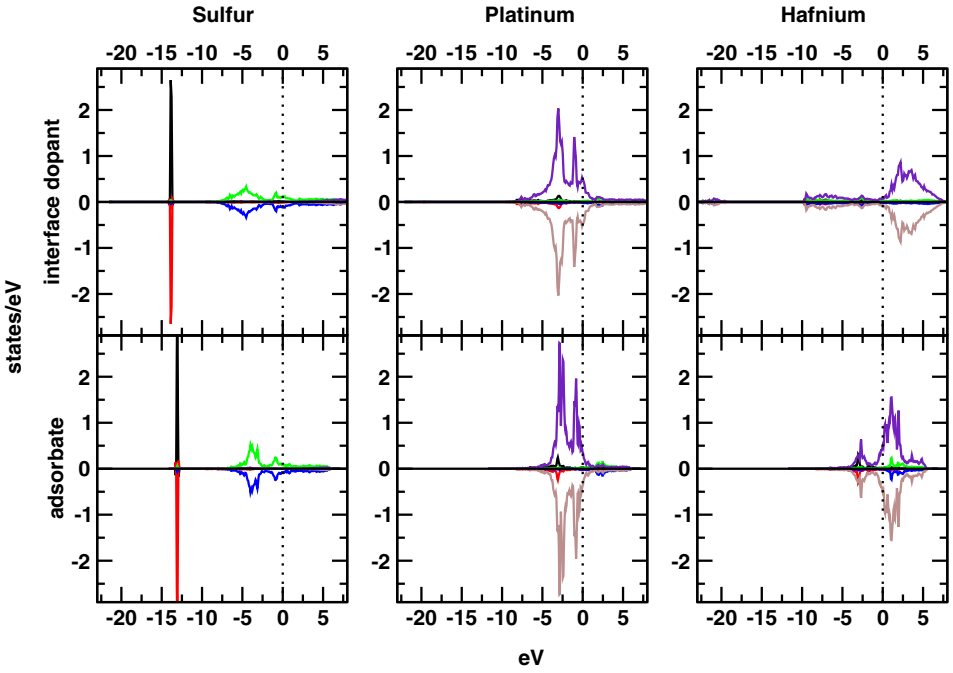

Fig. 6. Projected density of states for S, Pt and Hf. The top panels show the density of states when these atoms are in the interface. The bottom panels show the atoms as adsorbates on the NiAl(1 1 0) surface. Black is spin up s-states, red is spin down s-states, green is spin up p-states, blue is spin down p-states, indigo is spin up d-states, brown is spin down d-states. The vertical dotted line indicates the Fermi level. (For interpretation of the references to colour in this figure legend, the reader is referred to the web version of this article.)

as a substitutional impurity at the NiAl(1 1 0) surface. Hence we also carried out calculations akin to those described for the clean Al_2O_3(0 0 0 1)/NiAl(1 1 0) interface, but where we substituted one of the Ni atoms on the NiAl surface with a Pt atom. We considered two different locations for the Pt in the lateral unit cell, one where Pt substitutes for a Ni across from an oxygen atom in Al_2O_3 and one where Pt substitutes for a Ni across from an aluminum atom in Al_2O_3, in order to ensure our results accounted for both types of environments. Both structures were allowed to relax to optimal geometries, with the initial guesses for the structures taken to be that of the clean interface. Only small changes occur in cross-interface bonding upon Pt substitution. While some bonds lengthen, as one might expect due to the 0.14 Å larger radius of Pt compared to Ni, many Al–O and Al–Al cross-interface bonds actually shorten slightly, with all changes in bond lengths <0.1 Å. Hence, the number of cross-interface bonds stays roughly the same as well. As a result, the interfacial adhesion changes by less than 0.015 J m^{-2} compared to the unsubstituted interface, with the adhesion decreasing slightly for a Pt across from an oxygen atom in alumina (from 0.661 J m^{-2} in the clean interface down to 0.647 J m^{-2}) and increasing very slightly for a Pt across from an aluminum atom in alumina (0.672 J m^{-2}). However, these very small changes are likely to be within the error bars of our calculation and therefore we conclude that Pt substitution at the NiAl(1 1 0) surface does not affect the adhesion of alumina to NiAl. This further substantiates our conclusion that the role of Pt, whether it is a substitutional or interstitial impurity at the interface, is *not* to increase interfacial adhesion.

3.4. Hafnium-doped interface

As with the other segregating elements, we start with an initial structure where Hf is positioned in its predicted adsorption site on NiAl(1 1 0) [40], namely the Ni–Ni long-bridge site. Of the five possible Ni–Ni bridge sites, we again choose the site farthest away from all Ni–$Al_{Al_2O_3}$ cross-interface bonds. Again, an O atom from the oxide is nearly on top of the Hf in the initial guess structure before ion relaxation is allowed. We again acknowledge that other lower energy structures may exist, but for the same reasons as argued for S and Pt, we consider this possibility to be unlikely, and further exploration of other possible local minima was simply prohibitively expensive. Thus, we again regard the results presented below as representative of the properties of the doped interface, if not entirely definitive.

Unlike for S and Pt, the effect of Hf at the interface is most dramatic. In particular, we find that the ideal work of adhesion is three times larger than the adhesion of the clean interface! This increased interface stability is consistent with the fact that Hf is a dopant known to extend the lifetime of thermal barrier coatings [45]. The fully relaxed structure, shown in Fig. 1d, looks very different than the interface structures containing S or Pt. The Hf atom has moved toward the oxide, forming "bonds" with four oxygen atoms and retaining only one "bond" with the NiAl.

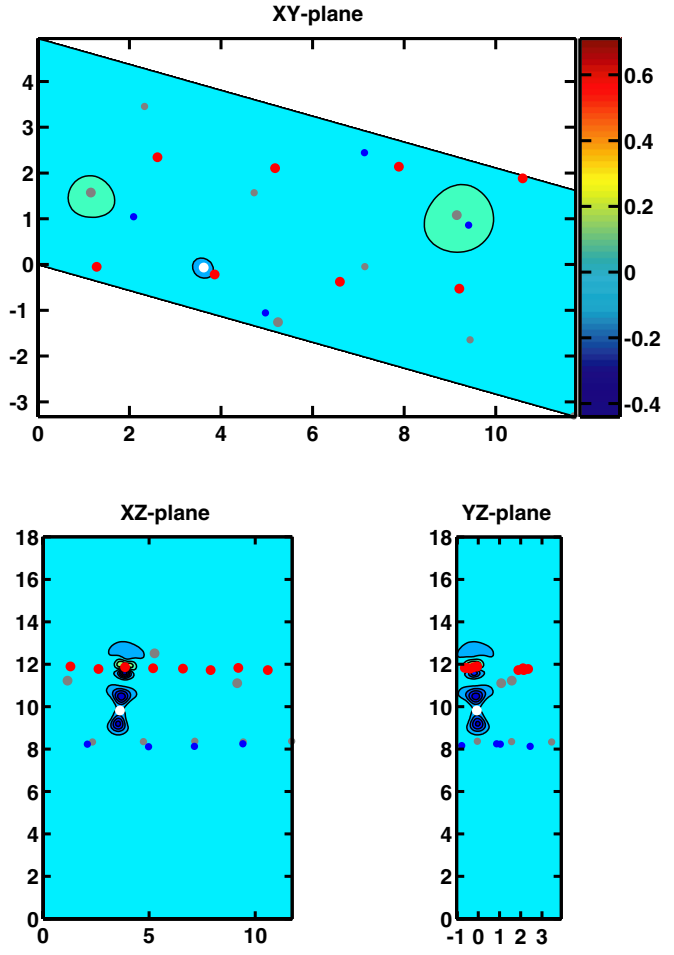

Fig. 7. Electron density difference maps for three cuts through the Al_2O_3/Pt/NiAl interface. The white dot marks the Pt atom. The dots mark the positions of the atoms in the oxide and substrate layers closest to the interface. Red is oxygen, blue is nickel, large grey is Al from the oxide, small grey is Al from the NiAl. The top panel shows the cut through the Pt atom parallel to the interface plane. The two lower panels show cuts perpendicular to the interface through the Pt atom. (For interpretation of the references to colour in this figure legend, the reader is referred to the web version of this article.)

The bond distances in Table 2 reveal Hf–O distances as short as 1.9 Å, which is much shorter than, e.g., the Hf–O distance in cubic HfO_2 (3.10 Å) [46,47]. Although the Hf–Ni and Hf–Al distances to the NiAl substrate are longer than for the other two segregating elements (Hf–Ni = 2.43 Å compared to Pt–Ni = 2.39 Å and S–Ni = 2.19 Å; Hf–Al = 2.78 Å compared to Pt–Al = 2.45 Å and S–Al = 2.37 Å), the gap between the metal and the oxide has decreased. This is evidenced by the Ni–Al cross-interface "bonds" shown in Fig. 1d and in the nearest-neighbor distances listed in Table 2. In particular, the Ni–$Al_{Al_2O_3}$ distances are nearly the same as in the clean interface, with three Ni–$Al_{Al_2O_3}$ distances shorter than 3 Å. Thus, even though a large dopant has been placed at this interface, the metal–oxide bonding in the clean interface is retained, concomitant with newly formed, strong Hf–O bonds. This bonding combination is probably the origin of the very strong adhesion of this doped interface.

In addition to the dramatic changes in position of the dopant atom, where Hf moves toward O and away from Ni (due to its high affinity for oxygen), we observe in Fig. 8 considerable rearrangement of the electron density around the Hf dopant and its oxide nearest neighbors. A significant depletion of electron density around the Hf atom occurs, with a corresponding electron density increase in the plane of the O atoms. Three of the four O atoms have a significant increase of density around them, with the largest increase around the O atom closest to the Hf. The rearrangement of density is apparent in all cuts

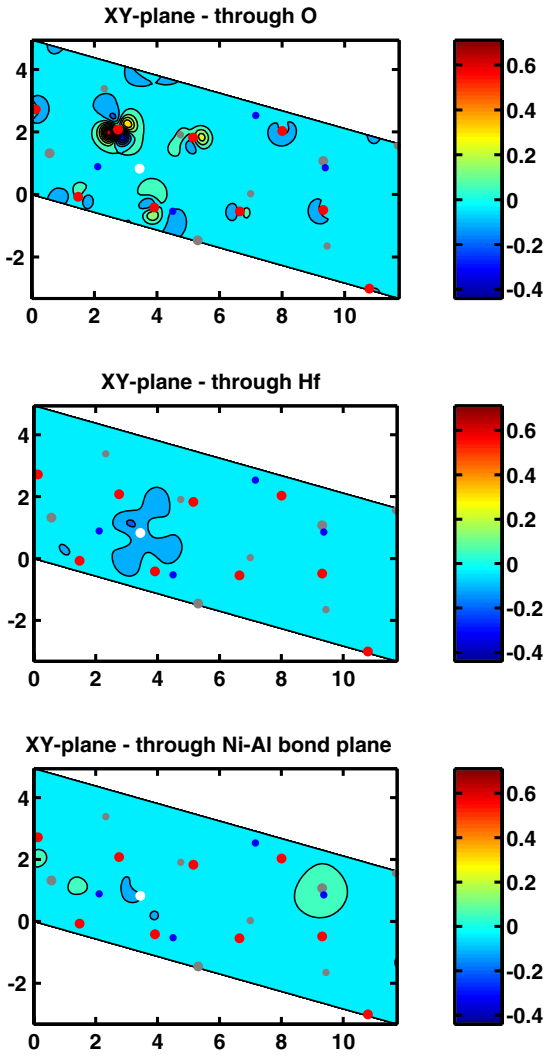

Fig. 8. Electron density difference maps for three cuts through the Al_2O_3/Hf/NiAl interface. The white dot marks the Hf atom. The dots mark the positions of the atoms in the oxide and substrate layers closest to the interface. Red is oxygen, blue is nickel, large grey is Al from the oxide, small grey is Al from the NiAl. The top panel shows the cut through the O atom closest to the Hf, and the middle panel shows the cut through the Hf atom, and the lower panel shows a cut through the Ni–$Al_{Al_2O_3}$ bond plane. All cuts are parallel to the interface plane. (For interpretation of the references to colour in this figure legend, the reader is referred to the web version of this article.)

shown of the Al_2O_3/Hf/NiAl interface. Hf's donation of electrons to the O atoms in alumina is consistent with the expected partially ionic/partially covalent nature of the bonding [25]. The bottom panel displays an increased density between a Ni atom and an Al atom from the oxide. This increase indicates that one of the bonds present in the clean interface is also present for the Hf-doped interface. Considering both the bond distance data in Table 2 and the charge density difference maps in Fig. 8, we conclude that at least six bonds formed across the interface (4 Hf–O, 1 Hf–Ni and 1 Ni–Al), which corresponds to a "bond density" of 10.1 bonds nm^{-2}. It is a matter of interpretation if Hf should be seen as belonging to the oxide or the metal substrate.

We also observe significant changes in the Hf LDOS when the alumina layer is present compared to the LDOS for Hf as an adsorbate on the NiAl(1 1 0) surface (see Fig. 6). The occupied Hf states as an adsorbate on NiAl(1 1 0) have all but disappeared at the interface, consistent with the charge transfer seen in the electron density difference maps. In Fig. 4 we see that the LDOS for the O atom closest to Hf exhibits a large downward shift in its occupied states, a further indication that charge has been transferred to this atom. By contrast, we see only very small changes in the Ni PDOS upon Hf addition to the clean interface. Thus, all indicators point to the conclusion that the strong adhesion of the NiAl/Hf/Al_2O_3 interface is due to the strong bonds formed between Hf and neighboring oxygens, which comprise the bridges between the two materials across the metal–oxide interface.

4. Discussion

Our characterization of the clean Al_2O_3/NiAl(1 1 0) interface is in line with earlier investigations. For example, STM and DFT studies of ultrathin films of alumina (with just two oxygen atom layers) on NiAl(1 1 0) found a strong preference for Al atoms in the oxide to occupy positions above the Ni rows of the NiAl(1 1 0) surface [41], just as we found here for three O atom layers of Al_2O_3. The gap between the metal and the ultrathin oxide film, expressed as the Ni–$Al_{Al_2O_3}$ distance, was determined to be 2.32 Å, similar to our Ni–$Al_{Al_2O_3}$ distance of 2.4 Å. Earlier DFT predictions of the oxide–metal distance and work of adhesion at the Al_2O_3/Ni(1 1 1) interface [36] are also similar to our findings: 2.32 Å and ~0.5 J m^{-2} for Al_2O_3/Ni vs. 2.4 Å and ~0.7 J m^{-2} for Al_2O_3/NiAl. The increased adhesion of alumina to the NiAl substrate compared to pure Ni may be attributed to the Al_{NiAl}–O cross-interface bonds that form in addition to the Ni–$Al_{Al_2O_3}$ bonds formed with both metal substrates. We also observe that the O atoms in Al_2O_3 at the clean interface try to adopt positions above NiAl(1 1 0) that are similar to the 2Al–Ni three-fold site favored for O atom adsorption on NiAl(1 1 0) [48]; the Al–O bond distance of 1.84 Å for O/NiAl(1 1 0) is also close to the Al–O distance of 2 Å across the alumina/NiAl interface predicted here. Thus, our optimized structure and adhesion of the clean oxide/metal interface is closely related to structures and adhesion determined previously, giving us confidence that this interface structure provides a trustworthy baseline for our studies of interfaces containing segregating elements.

The addition of even 0.1 ML of S at the metal/oxide interface is predicted to reduce the adhesion between Al_2O_3 and NiAl by almost 80%, to 0.18 J m^{-2}. This decrease in adhesion is connected with a clear reduction in the number of bonds across the interface and repulsion between S and O. For the clean interface, the "bond density" is 8.4 bonds nm^{-2}, but with S present at the interface, the "bond density" decreases to 1.7 bonds nm^{-2}. In addition, the gap between the metal and the oxide increases, e.g. the Ni–$Al_{Al_2O_3}$ distances are 2.86 Å or longer. The weakened adhesion and wider metal–oxide gap may explain the TEM measurements on TBCs that find S segregating to voids between the bond coat alloy and the oxide [8,7]. The elongated, weakened bonds we find across the S-containing metal/oxide interface and apparent S–O repulsion may induce the oxide and metal to separate and form voids upon experiencing stresses introduced during thermal cycling of the TBC.

The structure predicted for the Pt-doped interface is very similar to that found for S. However, the adhesion with Pt present is significantly larger than with S, although it is still 20% lower than the adhesion of the clean interface. The cross-interface bond density is lower than the clean interface and the metal–oxide gap is almost as large as for S, which certainly indicates a somewhat destabilized interface. Since the adhesion is stronger than for the S impurity, we conclude that the bonds that form between the metal and the oxide through Pt must be stronger. If we look closely at the structure of the Pt-containing interface, we find that Pt is positioned more in the middle of the interface, while S is closer to the metal side of the interface, consistent with the repulsion between S and O. Pt appears to promote Ni–$Al_{Al_2O_3}$ bond formation across the interface. Although the shortest distance between such a pair of atoms is longer than for S, the electron density difference maps exhibit density changes indicative of bond formation between two Ni–$Al_{Al_2O_3}$ pairs. Thus Pt manages to maintain adhesion similar to the clean interface. As mentioned earlier, it is known that bond coat alloys based on NiPtAl improve TBC lifetime [2], and it has been suggested that this is due to an increased resistance to scale spallation [49]. Our results rule out a direct role for Pt in improving adhesion of the metal/oxide interface. Instead, other mechanisms that have been suggested for Pt's role, such as inhibiting S segregation to the interface [15] or inhibiting growth of brittle spinels [45] are likely operating and demand further investigation.

There is a remarkable improvement in the ideal work of adhesion when Hf is present at the interface. Previous theoretical work had predicted that early transition metals such as Ti and Zr would improve the work of adhesion for the interface between Ni and Al_2O_3 by up to a factor

of two at high concentrations (0.5 ML) [35]. Here we find that Hf increases the metal–oxide adhesion even more, by a factor of three, even at low concentrations (0.1 ML)! Thus, one role for Hf as a dopant in TBCs is indeed a direct and dramatic increase in the intrinsic adhesive strength of the bond coat alloy/thermally grown oxide interface. The strong adhesion of the Ti- and Zr-doped Al_2O_3/Ni interface and that of the Hf-doped Al_2O_3/NiAl interface is correlated with formation of several strong bonds between the dopant and oxygen in alumina. In all three cases, the metal–oxide distance is quite short and similar to the gap for the clean interface. Hf occupies a position close to the oxide, making bonds with at least two oxygen atoms, and the metal–oxide gap is nearly unchanged from the clean interface. That Hf, an early transition metal with an open shell structure, improves adhesion was not particularly surprising [50], in light of the intrinsically strong bonds that form between early transition metal atoms and oxygen atoms. The open *d*-shell character of the early transition metals allows a mixture of ionic, covalent and donor–acceptor character to prevail in these metal-oxo bonds, which make them particularly strong [25]. It is clear that the stark increase in the work of adhesion is due largely to the change in cross-interface bond character, since the "bond density" increase compared to the clean interface is only about 25% (from $\sim$8 to $\sim$10 bonds nm^{-2}).

5. Conclusions

We have investigated how S impurities and Pt and Hf dopants affect the nature of the interface between close-packed surfaces of α-alumina and β-NiAl. The latter interface serves as a model for the weak link in TBCs, namely, the TGO/metal bond coat alloy interface. We find that S greatly weakens the alumina/NiAl interface, consistent with post-mortem TEM measurements that find void formation at the TGO/bond coat alloy interface correlates with the presence of sulfur. We also predict that metal–oxide adhesion is strongly dependent upon the relative lateral translation of the oxide with respect to the metal substrate. Adhesion for an unfavorable translation is more or less zero, or even slightly repulsive. Under typical operating conditions, thermal cycling of the TBC exposes the oxide to expansion and contraction cycles that introduce stresses due to the mismatch in coefficients of thermal expansion between alumina and the bond coat alloy. These thermal (and oxide growth) stresses can make poorly matched metal–oxide interfaces end up as weak spots for initiating voids that eventually develop into cracks that in turn will cause the TBC to spall. We find that adding Pt to the interface does not improve the intrinsic interfacial adhesion, thus excluding improved adhesion as a role for Pt in improving TBC lifetimes. By contrast, even small amounts of Hf produce a dramatic increase in adhesion, due to strong new bonds forming between the metal and the oxide through the dopant, concomitant with retention of the original metal–oxide bonding of the clean interface. Thus, at least one function of Hf in extending TBC lifetimes is a very large increase in the stability of the thermally grown oxide/bond coat alloy interface as a result of Hf addition. Other roles that Hf and Pt may play in TBCs are currently under investigation.

Acknowledgement

We are grateful to the Air Force Office of Scientific Research (AFOSR) for funding of personnel and computing time at the Maui High Performance Computing Center (MHPCC).

References

[1] Demaray RE, Halnan WK, Shan S. Development of electron beam physical vapor deposition of ceramic coatings, EPRI RD-2369-SR; May 1982, p. 6–184.
[2] Goward GW. Progress in coatings for gas turbine airfoils. Surf Coat Technol 1998;108–109:73.
[3] Rabiei A, Evans AG. Failure mechanisms associated with the thermally grown oxide in plasma-sprayed thermal barrier coatings. Acta Mater 2000;48:3963.
[4] Wright PK, Evans AG. Mechanisms governing the performance of thermal barrier coatings. Curr Opin Solid State Mater Sci 1999;4:255.
[5] Hohenberg P, Kohn W. Inhomogenous electron gas. Phys Rev 1964;136(3B):B864.
[6] Kohn W, Sham LJ. Self-consistent equations including exchange and correlation effects. Phys Rev 1965;140(4A):A1133.
[7] Brady MP, Pint BA, Tortorelli PF, Wright IG, Hanrahan Jr RJ. High-temperature oxidation and corrosion of intermetallics. In: Schültze M, editor. Corrosion and environmental degradation – volume ii (materials science and technology – a comprehensive treatment). Weinheim: Wiley-VCH; 2000. p. 229–325.
[8] Grabke HJ. Surface and interface segregation in the oxidation of metals. Surf Interface Anal 2000;30:112.
[9] Smialek JL, Jayne DT, Schaeffer JC, Murphy WH. Effects of hydrogen annealing, sulfur segregation and diffusion on the cyclic oxidation resistance of superalloys: a review. Thin Solid Films 1994;253:285.
[10] Zhang Y, Lee WY, Haynes JA, Wright IG, Pint BA, Cooley KM, et al. Synthesis and cyclic oxidation behavior of a (Ni,Pt)Al coating on a desulfurized Ni–base superallloy. Metal Mater Trans A 1999;30A:2679.
[11] Gaudette FG, Suresh S, Evans AG. Effects of sulfur on the fatigue and fracture resistance of interfaces between γ-Ni(Cr) and α-Al_2O_3. Metal Mater Trans A 2000;31A:1977.
[12] Haynes JA, Lance MJ, Pint BA, Wright IG. Characterization of commercial EB-PVD TBC systems with CVD (Ni,Pt)Al bond coatings. Surf Coat Technol 2001;146:140.
[13] Evans AG, Mumm DR, Hutchinson JW, Meier GH, Pettit FS. Mechanisms controlling the durability of thermal barrier coatings. Prog Mater Sci 2001;46:505.
[14] Pint B. Experimental observations in support of the dynamic-segregation theory to explain the reactive-element effect. Oxide Met 1996;45:1.
[15] Zhang Y, Haynes JA, Lee WY, Wright IG, Pint BA, Cooley KM, et al. Effects of Pt incorporation on the isothermal oxidation behavior chemical vapor deposition aluminide coatings. Metal Mater Trans A 2001;32A:1727.
[16] Han X, Zhang Y, Xu H. First-principles calculation on adhesions of Ni/Al_2O_3 and Ni/ZrO_2 interfaces. Chem Phys Lett 2003;378:269–72.
[17] Brickey MR, Lee JL. Structural and chemical analyses of a thermally grown oxide scale in thermal barrier coatings containing a platinum–nickel–aluminide bond coat. Oxide Met 2000;54:237.

[18] Pint BA, Wright IG, Lee WY, Zhang Y, Prüssner K, Alexander KB. Substrate and bond coat compositions: factors affecting alumina scale adhesion. Mater Sci Eng A 1998;A245:201.
[19] Svensson H, Angenete J, Stiller K, Langer V. Microcstructural studies of NiAl-based model alloys and commercial coatings after isothermal oxidation. Mater High Temp 2003;20:421–8.
[20] Pint BA, Wright IG, Brindley WJ. Evaluation of thermal barrier coating systems on novel substrates. J Therm Spray Technol 2000;9:198.
[21] Rhouta B, Pieraggi B. Microstructural characterization of the oxide scale grown at the interface between PSZ top coat and MCrAlY bond coat. Mater Sci Forum 2001;369–372:687.
[22] Schulz U, Menzebach M, Leyens C, Yang YQ. Influence of substrate material on oxidation behavior and cyclic lifetime of EB-PVD TBC systems. Surf Coat Technol 2001;146:117.
[23] Mennicka C, He M-Y, Clarke DR, Smith JS. The role of secondary oxide inclusions (''Pegs'') on the spalling resistance of oxide films. Acta Mater 2000;48:2941.
[24] Jarvis EA, Carter EA. Phys Rev B 2002;66:100103(R).
[25] Jarvis EAA, Carter EA. J Phys Chem B 2002;106:7995–8004.
[26] Nicholls JR. Designing oxidation-resistant coatings. JOM 2000;52:28.
[27] Kresse G, Hafner J. Ab initio molecular dynamics for open-shell transition metals. Phys Rev B 1993;48(17):13115.
[28] Kresse G, Furthmüller J. Efficient iterative schemes for ab initio total-energy calculations using a plane-wave basis set. Phys Rev B 1996;54(16):11169.
[29] Kresse G, Furthmüller J. Efficiency of ab initio total energy calculations for metals and semiconductors using a plane-wave basis. Comput Mater Sci 1996;6(1):15.
[30] Perdew JP, Burke K, Ernzerhof M. Phys Rev Lett 1996;77:3865. erratum: Phys Rev Lett 1997;78:1396.
[31] Blöchl PE. Projector augmented-wave method. Phys Rev B 1994;50(24):17953.
[32] Kresse G, Joubert J. From ultrasoft pseudopotentials to the projector augmented wave method. Phys Rev B 1999;59(3):1758.
[33] Monkhorst HJ, Pack JD. Special points for Brillouin-zone integrations. Phys Rev B 1976;13(12):5188.
[34] Guo J, Ellis DE, Lam D. J Phys Rev B 1992;45:13647.
[35] Jarvis EAA, Carter EA. J Phys Chem B 2001;105:4045.
[36] Jarvis EAA, Christensen A, Carter EA. Surf Sci 2001;487:55.
[37] Clausen Jr EM, Hren JJ. Mater Res Soc Symp Proc 1985;41:381–6.
[38] De-en Jiang, private communication.
[39] Jarvis EAA, Carter EA. Comput Sci Eng 2002;4:33.
[40] Carling KM, Glover W, Gunaydin H, Mitchell TA, Carter EA. Comparison of S, Pt, and Hf adsorption on NiAl(110). Surf Sci 2006;600:2079.
[41] Kresse G, Schmid M, Napetschnig E, Shishkin M, Köhler L, Varga P. Structure of the ultrathin aluminum oxide film on NiAl(110). Science 2005;308:1440.
[42] Kuczkowski, Suenram, Lovas. Microwave spectra, structure, and dipole moment of sulfuric acid. J Am Chem Soc 1981;103:2561–6.
[43] Lin Xi, Ramer NJ, Rappe AM, Hass KC, Schneider WF, Trout BL. Effect of particle size on the adsorption of O and S atoms on Pt: a density-functional theory study. J Phys Chem B 2001;105: 7739–47.
[44] Jiang C, Besser MF, Sordelet DJ, Gleeson B. A combined first-principles and experimental study of the lattice site preference of Pt in B2 NiAl. Acta Mater 2005;53:2101.
[45] Pint BA, More KL, Wright IG. Effect of quarternary additions on the oxidation behaviour of Hf-doped NiAl. Oxid Met 2004;59:257.
[46] Foster AS, Lopex Gejo F, Shluger AL, Nieminen RM. Phys Rev B 2002;65:174117.
[47] Zhao X, Vanderbilt D. Phys Rev B 2002;65:233106.
[48] Lozovoi AY, Alavi A, Finnis MW. Phys Rev Lett 2000;85:610.
[49] Wright IG, Pint BA. Bond coating issues on thermal barrier coatings for industrial gas turbines. Proc IMechE 2005;219:101.
[50] Carter EA, Goddard III WA. Early- versus late-transistion-metal-oxo bonds: the electronic structure of VO^+ and RuO^+. J Phys Chem 1988;92:2109.